

УДК 519.622

КВАЗИТРЕХМЕРНАЯ МОДЕЛЬ ТОПЛИВНЫХ ЭЛЕМЕНТОВ С ПОЛИМЕРНЫМ ЭЛЕКТРОЛИТОМ

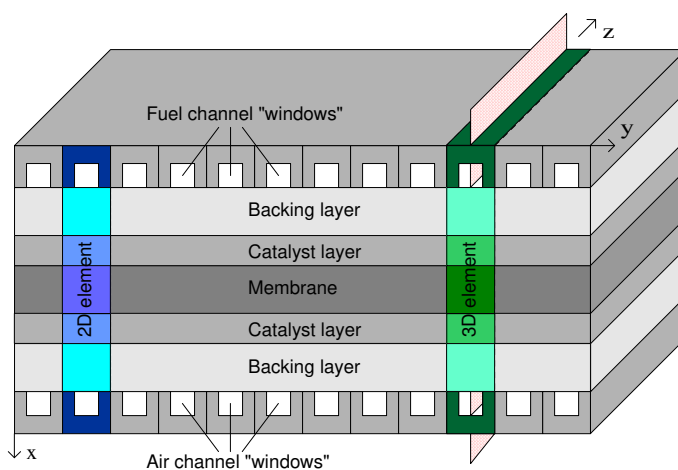
А. А. Куликовский¹

Описана квазитрехмерная модель топливных элементов с полимерным электролитом. Модель основана на уравнениях переноса газа в топливных каналах и пористых слоях, уравнениях сохранения тока и Батлер–Вольмеровских формулах для скоростей электрохимических реакций. Модель описывает каталитические слои и дает “карты” распределения параметров в сечении топливного элемента с длинными топливными каналами на обеих сторонах. В качестве примера продемонстрирована роль транспорта воды. Показано, что вблизи входа в канал электроосмотический эффект может заметно осушать анодный каталитический слой и соседние участки мембраны, что ухудшает эффективность работы элемента.

Ключевые слова: топливные элементы, квазитрехмерные модели, полимерный электролит, уравнения сохранения тока, электрохимические реакции, каталитический слой.

1. Introduction. Polymer electrolyte fuel cells (PEFCs) are expected to perform a revolution in many areas of power engineering. Environmental friendly PEFC-based stationary and mobile power sources (including vehicles) are anticipated to replace old-fashioned classical power sources (batteries and diesel engines). During the past decade, the power density of hydrogen PEFCs has been grown up to $\approx 1 \text{ W cm}^{-2}$ with the concurrent 10-fold decrease of precious metal loading [1].

The heart of a PEFC is the membrane–electrode assembly (MEA): two gas diffusion (backing) layers and two catalyst layers separated by a membrane. The MEA is usually clamped between metal current collectors that have channels for the feed gas supply (Figure 1).



Sketch of a fuel cell and the system of coordinates. Flow fields are formed by two meander channels on both sides. The cell cross section consists of geometrically identical 2D elements. Along-the-channel models give the map of parameters in a red plane. The fully 3D model deals with just a short piece of a cell (3D element), whereas our quasi-3D model gives a map of parameters in a whole cross section

The feed gases (hydrogen at the anode and oxygen at the cathode) are supplied to the respective channels. Then the gases diffuse through the backing layers and reach the respective catalyst layer. Hydrogen is ionized in the anode catalyst layer yielding protons. The protons move through the polymer electrolyte membrane to

¹ Научно-исследовательский вычислительный центр, Московский государственный университет им. М. В. Ломоносова, 119992, Москва; e-mail: akul@srcc.msu.su

the cathode catalyst layer, where they are consumed in the oxygen reduction reaction. The current of protons in the membrane causes the current of electrons in the external load.

The electrochemical reactions in the anode and the cathode catalyst layers are



so that the only byproduct is water.

Several difficulties still hamper a wide distribution of PEFCs. The most essential are

- poor kinetics of the oxygen reduction reaction,
- poisoning of the anode catalyst layer by CO, which is a byproduct of hydrocarbon fuel reforming,
- flooding of the cathode catalyst layer by water produced in the electrochemical reaction, which blocks the delivery of oxygen to the catalyst sites.

Modeling helps to clarify the physics of the PEFC operation and gives useful hints how to improve the cell performance and design. During the past decade, a number of sophisticated 2D models were developed (Fuller and Newman [2], Nguyen and White [3], Yi and Nguyen [4], Dannenberg, Ekdunge and Lindbergh [5], Um, Wang and Chen [6], Futerko and Hsing [7, 8], Wang, Wang and Chen [9], Natarajan and Nguyen [10]).

These models give a map of parameters in a cross section of MEA either in a single 2D element in the (x, y) plane (across-the-channel models, Figure 1) or in the (x, z) plane (along-the-channel models, Figure 1). Each type of models ignores a distribution of parameters in the “other” plane.

The common belief is that the most detailed information give fully three-dimensional (F3D) models. The complexity of F3D modeling of fuel cells stems from their geometry: the cell is a two-scale system. The channel for the feed gas supply can be up to several meters long, whereas the MEA thickness is about several hundreds micrometers (i.e., the ratio of these values is about 10^3 – 10^4). Because of evident computer limitations, the unique F3D model of Dutta, Shimpalee, and Van Zee [11] allows one to simulate only a small part of the cell, which includes a 10-cm fragment of the channel (3D element, Figure 1). The large-scale effects induced by the feed gas exhaustion and water accumulation in a long channel are out of the scope of the F3D models.

However, this two-scale nature of the fuel cell allows one to develop an efficient quasi-3D (Q3D) model, as described below. This model gives a map of parameters in the cross section of a cell equipped with channels up to several meters long. The feature of the Q3D model is its ability to describe the nonlinear interplay between large and small-scale effects.

In the first version of the Q3D model it was assumed that the membrane is fully hydrated and its conductivity is constant [12, 13]. This assumption applies the evident restriction: the effects of partial membrane drying cannot be described. In this paper we present a complete formulation of the current version of the extended Q3D model, which takes into account water transport in a fuel cell ¹.

As an example of capabilities of the model, we present some results of simulation of PEFCs equipped on both sides with long (≈ 40 cm) channels. The model allows one to locate dry regions, which make the main contribution to the membrane resistance.

2. The model.

2.1. General description. Consider a PEFC equipped on both sides with meander-like channels. Our aim is to obtain a distribution of parameters in the cross section shown in Figure 1.

This cross section consists of a number of geometrically identical (or similar) 2D elements (Figure 1). The adjacent elements are connected by segments of the channels. The main idea of the Q3D model is as follows. A variation of feed gas concentration in the channels on a length of the order of the MEA thickness is usually small ². This allows one to neglect the z -component of currents and fluxes in porous layers and in the membrane. The 3D problem can then be split into a 2D problem in a cell cross section (the internal problem) and a problem of gas flow in the channel (the channel problem). Both the problems are coupled via the mean current density (the local current density) in each element.

The flow in the channel can be described by models of various complexity; the simplest is a 1D formulation. Consider the oxygen side of the cell. Oxygen is consumed in the electrochemical reaction; the continuity equation for oxygen concentration, hence, contains a term proportional to the local current density $j(z)$. For given $j(z)$,

¹This version of the model was used to simulate recent experiments of Büchi and Scherer [14].

²More accurate, this is the case if $l_{\text{MEA}} \ll L_1$, where l_{MEA} is the MEA thickness and L_1 is the characteristic length of feed gas consumption. Using the expression for L_1 [15], we get $\frac{S}{nF} \frac{l_{\text{MEA}} l_c i_*}{h\nu c_{\text{ref}}} \exp\left(\frac{\alpha F}{RT} \eta\right) \ll 1$. The smallness of the left-hand side is provided by the product $l_{\text{MEA}} l_c$. For very large overpotentials (for large mean current densities), this condition fails. Physically this means that all fuel is consumed very close to the inlet. We, however, will assume that this is not the case.

one can calculate the oxygen concentration in each “window” shown in Figure 1. Using these concentrations as boundary conditions, one can solve the internal problem and calculate a new profile $j(z)$ ³. This procedure is repeated until the convergence is reached.

The advantage of this approach is that it enables an effective parallelization. The internal problem is formulated for a single element, and each element then “is solved” on a separate processor. Upon completion of the iteration step, adjacent elements exchange boundary conditions, as described below. This allows one to simulate cells with an arbitrary number of elements (i.e., with arbitrary long channels).

2.2. The internal problem.

2.2.1. Main assumptions. The main physical assumptions are as follows:

- the membrane is impermeable to feed gases;
- any fluxes due to the temperature gradient are negligible;
- the flux of gas components in porous (backing and catalyst) layers is caused by the pressure gradient (if any) and by diffusion due to the concentration gradient;
- the contribution of liquid water to the mass balance on both sides of the cell is negligible;
- reaction rates on both sides of the cell can be described by the Butler–Volmer equations.

These assumptions are discussed in detail in [13].

2.2.2. Gases flow. The system of coordinates is shown in Figure 1 (the x -axis is directed across the cell, the z -axis is directed along the channel, and the y -axis is directed parallel to the cell surface). The molar flux of the i th gas component is

$$\mathbf{N}_i = -cD_i\nabla\xi_i + c\xi_i\mathbf{v}^{D'Arcy}, \quad (3)$$

where c is the total molar concentration of a mixture, D_i is the effective diffusion coefficient, ξ_i is the molar fraction of the i th component, and $\mathbf{v}^{D'Arcy}$ is the D'Arcy velocity given by

$$\mathbf{v}^{D'Arcy} = -\frac{k^p}{\mu}\nabla p. \quad (4)$$

Here k^p is the hydraulic permeability of the porous layer and μ is the gas viscosity. Physically, relation (4) means that the pressure gradient induces the Poiseuille flow in pores.

Estimates show that in the absence of the pressure gradient, the Knudsen diffusion dominates in catalyst layers and the free molecular diffusion is the main mechanism of the gas transport in backing layers. The effective diffusion coefficient D_i interpolates between the Knudsen diffusion coefficient D_i^K in the catalyst layer

$$D_i^K = \psi\bar{r}\sqrt{\frac{8RT}{\pi M_i}} \quad (5)$$

and the mean free molecular diffusion coefficient D_i^b in the backing layer

$$\frac{\varepsilon^B}{D_i^b} = \sum_j \frac{\xi_j}{D_{ij}}. \quad (6)$$

Here \bar{r} is the mean pore radius in the catalyst layer, ψ is the correction for porosity in the catalyst layers, D_{ij} is the binary diffusion coefficient [16], and ε^B is the Bruggemann correction for porosity in the backing layers.

On the anode side the interpolation has the form

$$D_i = D_i^b + (D_i^K - D_i^b) \frac{1}{2} \left(1 - \tanh \left(\frac{x - x_0}{\Delta_0} \right) \right). \quad (7)$$

Here x_0 is the coordinate of the backing/catalyst layer interface and Δ_0 is the thickness of the transition region. At the cathode side, (7) must be modified to get the “mirror” function along x .

The mass conservation of the i th component reads as

$$\nabla \cdot \mathbf{N}_i = \frac{S_i}{nF} Q, \quad (8)$$

where Q is the Butler–Volmer rate of the electrochemical reaction (see below), S_i is the stoichiometry coefficient, and n is the number of electrons participating in the reaction. Outside the catalyst layers $Q = 0$.

³The latter is obtained by linear interpolation of values in windows.

Substituting (3) and (4) into (8), we get an equation for ξ_i which contains the pressure gradient. The equation for pressure follows from the following arguments. Neglecting the mass of protons, we can suppose that in the MEA there are no volume sources of total mass, i.e.,

$$\nabla \cdot (\rho \mathbf{v}^{D'Arcy}) = 0.$$

Taking into account (4) and the gas law $p = \frac{\rho}{M} RT$, we get

$$\nabla \cdot \left(\frac{M}{RT} p \nabla p \right) = 0. \quad (9)$$

Here M is the total molecular weight of the gas mixture given by $M = \sum_i \xi_i M_i$.

Since the membrane is impermeable to gases, equations (8) and (9) can be formulated for each side of the cell separately. Water is transported through the membrane and, hence, requires a special treatment.

2.2.3. Transport of water. It is convenient to formulate an equation for the molar concentration of water c_w rather than for the molar fraction. The flux of water in backing layers (3) is then

$$\mathbf{N}_w = -D_w \nabla c_w + c_w \mathbf{v}^{D'Arcy}, \quad (10)$$

where D_w is calculated with (7).

The water flux in the membrane is

$$\mathbf{N}_w = -D_w^m \nabla c_w + n^d \frac{\mathbf{j}}{F}, \quad (11)$$

where \mathbf{j} is the local proton current density. The second term in (11) describes the water transport due to the electroosmotic effect (the drag coefficient n^d is the number of water molecules transported by a proton). The first term is the diffusion due to the concentration gradient. Note that D_w^m depends on the water content in the membrane, which makes the problem nonlinear.

The catalyst layer is partially filled with electrolyte and has voids for the diffusion gas transport. The water flux in the catalyst layer is thus a combination of (10) and (11). Let ε be a volume fraction of electrolyte in the catalyst layer; the water flux then is

$$\mathbf{N}_w = -D_w^K \nabla c_w + \varepsilon \left(-D_w^m \nabla c_w + n^d \frac{\mathbf{j}}{F} \right). \quad (12)$$

Note that D_w^K (see (5)) takes into account a fraction of voids in the catalyst layer.

In the cathode catalyst layer water is produced. In other layers water is not produced neither consumed. The mass conservation equation for water, therefore, reads as

$$\nabla \cdot \mathbf{N}_w = \frac{S_w}{nF} Q_c, \quad (13)$$

where Q_c is the rate of the electrochemical reaction in the cathode catalyst layer (zero outside this layer). Equation (13) with fluxes (10), (12), and (11) gives equations for water concentration in the backing layer, in the catalyst layer, and in the membrane, respectively.

2.2.4. Potentials. Physically, the electrochemical reactions occur in the high electric field of a double layer, which exists at the metal/electrolyte interface. In the porous catalyst layer, the double layer forms a complicated tortuous structure. In the fuel cell simulations, this structure is modeled by continuous distributions of two potentials: φ , the potential of carbon threads (which interconnect catalyst particles) and φ_m , the potential of polymer electrolyte (the membrane phase), which provides transport of protons to catalyst sites. The difference between these potentials (overpotential) determines the rate of electrochemical reactions (see Section 2.2.5).

The potentials φ_m and φ are governed by the proton and electron current conservation equations, respectively:

$$\nabla \cdot (\sigma_m \nabla \varphi_m) = \begin{cases} -Q_a & \text{in the anode catalyst layer,} \\ Q_c & \text{in the cathode catalyst layer,} \\ 0 & \text{otherwise,} \end{cases} \quad (14)$$

$$\nabla \cdot (\sigma_a \nabla \varphi_a) = \begin{cases} Q_a & \text{in the anode catalyst layer,} \\ 0 & \text{otherwise,} \end{cases} \quad (15)$$

$$\nabla \cdot (\sigma_c \nabla \varphi_c) = \begin{cases} -Q_c & \text{in the anode catalyst layer,} \\ 0 & \text{otherwise,} \end{cases} \quad (16)$$

where σ_m is the membrane phase conductivity and σ_a, σ_c are the carbon phase conductivity on the anode and on the cathode side, respectively.

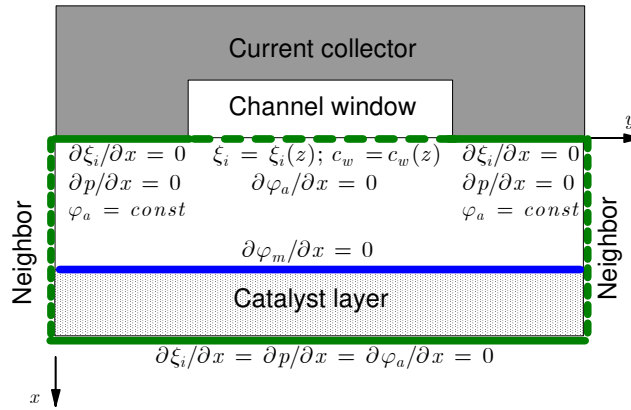
2.2.5. Reaction rates. Electrochemical reactions in fuel cells are multistage processes, in which certain stages may or may not depend on the overpotential. In our model we employ the Butler–Volmer relations for the rates of hydrogen ionization and oxygen reduction:

$$Q_a = i_a^* \frac{c_{\text{H}_2}}{c_{\text{H}_2 \text{ ref}}} \left[\exp\left(\frac{\alpha_a F}{RT} \eta_a\right) - \exp\left(-\frac{\alpha_a F}{RT} \eta_a\right) \right], \quad (17)$$

$$Q_c = i_c^* \frac{c_{\text{O}_2}}{c_{\text{O}_2 \text{ ref}}} \left[\exp\left(\frac{\alpha_c F}{RT} \eta_c\right) - \exp\left(-\frac{\alpha_c F}{RT} \eta_c\right) \right]. \quad (18)$$

Here Q is the number of protons produced/consumed per unit volume per unit time, i^* is the exchange current density (per unit volume), c_{ref} is the reference molar concentration of the feed gas, α is the transfer coefficient, and subscripts “a” and “c” refer to the anode and to the cathode sides, respectively. Overpotentials are defined as $\eta_a = \varphi_a - \varphi_m$ and $\eta_c = \varphi_m - \varphi_c$ (both are positive along with Q_a and Q_c).

Our aim is to capture 3D effects; the Butler–Volmer relations give a simple but physically realistic approximation of reaction rates. This allows a transparent interpretation of the results in terms of the two parameters i^* and α . At this stage of Q3D modeling, there is no need in more sophisticated reaction schemes, since this would just complicate the analysis.



The boundary conditions for the anode side of a single 2D element shown in Figure 1. Similar conditions are imposed on the cathode side

2.2.6. Boundary conditions. Boundary conditions for the anode side of a single element are shown in Figure 2. At the current collector/backing layer interface (solid green line), the potential is fixed and the normal (x -) component of all fluxes is zero. At the channel/backing layer interface (dashed green line), the molar fraction of gases and the concentration of water are obtained from the channel problem. Along the backing layer/catalyst layer interface (blue line), the normal proton current is zero. Along the catalyst layer/membrane interface (solid green line at the bottom), the normal components of all fluxes (except water) are zero.

The mass balance equations for water are solved separately in (i) the backing and catalyst layers and (ii) in the membrane. At the catalyst layer/membrane interface, the continuity of the normal component of the water flux and of the water molar concentration is used as a boundary condition (the details will be published in [17]).

2.3. The channel problem. The laminar steady flow in a long channel with impermeable walls basically is a Poiseuille flow with a constant velocity determined by the pressure gradient. Due to electrochemical reactions, however, the velocity in the channel of a fuel cell varies. A one-dimensional model of gas flow in the channel which takes into account the mass and momentum transfer through the channel/backing layer interface was developed in [18]. It shows that the flow in the channel can be treated as incompressible. The velocity distribution then is obtained from a mass balance equation. In the cathode channel this equation reads as

$$\rho^0 \frac{\partial v}{\partial z} = \frac{j(z)}{h} \frac{[2(1+2a)M_w - M_{\text{O}_2}]}{4F}, \quad (19)$$

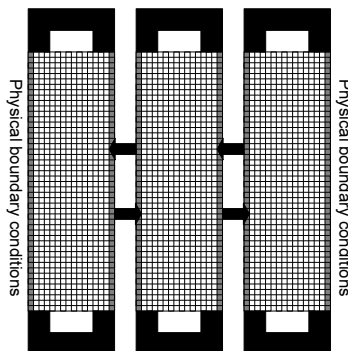
where ρ^0 is the flow density (constant), v is the flow velocity, h is the channel height, M is the molecular weight, and a is the effective coefficient of water transport through the membrane [18]. The latter is defined as the

number of water molecules transported from the anode to the cathode per each proton. Note that a coincides with the drag coefficient n^d only when the diffusion flux of water in the membrane is negligible.

Under a given $j(z)$, equation (19) determines the profile of velocity $v(z)$. The continuity equation for oxygen

$$\frac{\partial(c_{O_2}v)}{\partial z} = -\frac{j(z)}{h4F} \tag{20}$$

then gives the profile of oxygen molar concentration $c_{O_2}(z)$. Similar equations are written for hydrogen in the anode channel.



The scheme of exchanges between adjacent elements for the case when the cell cross section consists of just three elements. At each iteration step, every element exchanges “boundary conditions” (values of all variables along vertical columns) with its neighbors. The physical boundary conditions are formulated only at the left side of the leftmost element and at the right side of the rightmost element

3. Numerical aspects. Mass balance equations (8) and (13) with fluxes (3) and (11) respectively lead to convection–diffusion equations of the type

$$\nabla \cdot (-D\nabla u + \mathbf{W}u) = q, \tag{21}$$

where D is the diffusion coefficient and \mathbf{W} is the “convective” velocity. The feed gas concentrations in backing and catalyst layers are determined by (21) with $D = D(\mathbf{r})$ (a function of coordinates). The water transport in the membrane and in the catalyst layers is governed by a nonlinear version of (21) with $D = D(u)$. Equations (14)–(16) formally have the form (21) with $W = 0$ and $D = \sigma$.

The internal model is formulated for a single 2D element (Figure 1). We introduce a rectangular grid that covers the computational domain (Figure 3). Equations (21) are converted to a finite-difference form with the method of control volume. In the case when $D = D(\mathbf{r})$, the fluxes through the surfaces of computational cells are calculated with the Scharfetter–Gummel scheme [19]. In the case when $D = D(u)$ (water in the membrane), the fluxes are calculated with a specially developed q -scheme [20]. The equations for potentials (14)–(16) are approximated on a 5-point computational molecule, as described in [21]. Equation (14) is subject to the Dirichlet boundary conditions (zero derivative) along both the backing/catalyst layer interfaces (Figure 2). The unique solution is selected by the condition that reactions on both sides of the cell produce/consume the same current (see [22] for details).

To accelerate convergence, the local Newton method is employed for each equation. In all cases this procedure leads to a system of linear algebraic equations, which is solved by a standard iteration procedure.

The $x \times y$ size of the grid for a single element typically is 100×200 . One of the largest advantages of the Q3D model is the possibility of effective parallelization.

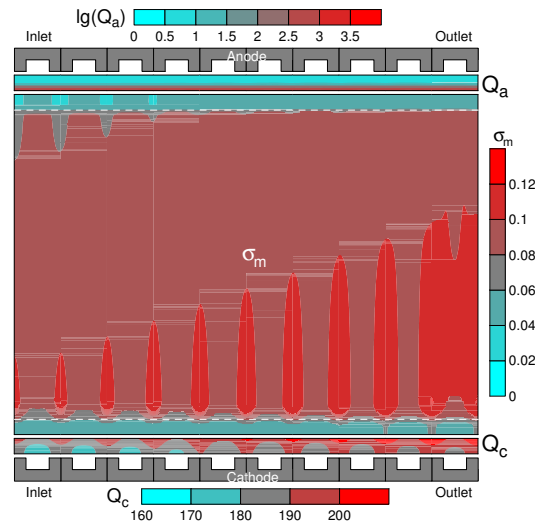
Let the along-the-channel profile of current density $j(z)$ is known (it is the same in both channels). The full iteration step consists of the following sub-steps.

1. For given $j(z)$, solve the channel problem for both the anode and cathode channels. This gives the gas concentrations in all channel windows (Figure 1);
2. Using these concentrations as boundary conditions, solve the internal problem for all 2D elements (Figure 1). The problem for each element is solved on a separate processor.
3. Exchange “boundary conditions” with adjacent elements (Figure 3).
4. Calculate a new $j(z)$.

Typical calculation requires 10–30 hours on a cluster of PC (based on 1 GHz Intel Pentium® processors). One more level of parallelism can be organized for solution of a system of linear equations. We implemented a parallel version of the well-known method of SOR with red–black ordering. It appeared that this method is rather expensive: the 2-fold increase in speed of calculations requires the 4-fold increase in the number of processors. However, in some cases this reserve is useful.

	Anode side	Cathode side
Cell temperature (C)	60	60
Inlet parameters:		
Gas pressure (Atm)	3.0	3.0
Inlet flow velocity (cm s ⁻¹)	30	30
Oxygen molar fraction		0.844
Water vapor molar fraction	0.156	0.156
Hydrogen molar fraction	0.844	
$c_{\text{O}_2 \text{ ref}}$ (mole cm ⁻³)		31.8×10^{-6}
$c_{\text{H}_2 \text{ ref}}$ (mole cm ⁻³)	56.4×10^{-6}	
i_* (A cm ⁻³)	1.4×10^5	1.0×10^{-5}
Transfer coefficient α	0.5	1.0
Reaction order γ	1.0	1.0
<hr/>		
Carbon phase conductivity ($\Omega^{-1} \text{ cm}^{-1}$)		40
Catalyst layer thickness (μm)		10
Backing layer thickness (μm)		100
Membrane thickness (μm)		200
Channel width (cm)		0.1
Channel height (cm)		0.1
Channel length (cm)		42.3

Conditions and parameters

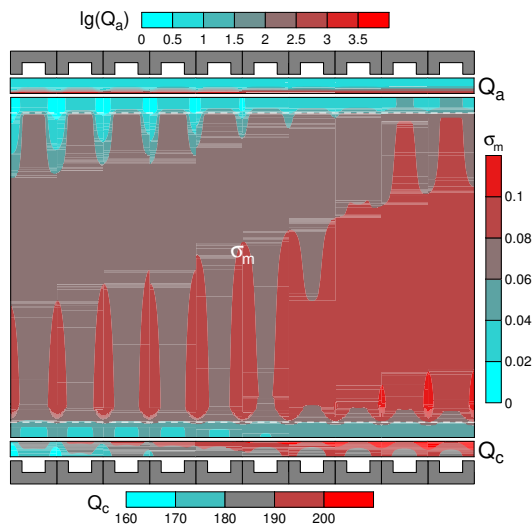


The maps of reaction rates Q_a and Q_c (A cm⁻³) and of membrane conductivity σ_m ($\Omega^{-1} \text{ cm}^{-1}$), including the membrane phase conductivity in catalyst layers. The catalyst layers/bulk membrane interface is shown by white dashed lines. Base set of parameters (Table 1), the mean current density is 200 mA cm⁻²

4. Results and discussion. The above model was used to simulate PEFCs equipped on both sides with single meander channels 42.3 cm long. Conditions and parameters for the base variant are shown in Table 1. The cell temperature is 60°C; the water concentration at the inlet of both the anode and cathode channels corresponds to the temperature of humidifier 80°C.

To clarify the influence of feed gas humidification on the cell performance, another simulation was performed for the cell with twice lower water concentration at the inlets of both the anode and cathode channels. This variant will be referred to as a “dry” cell.

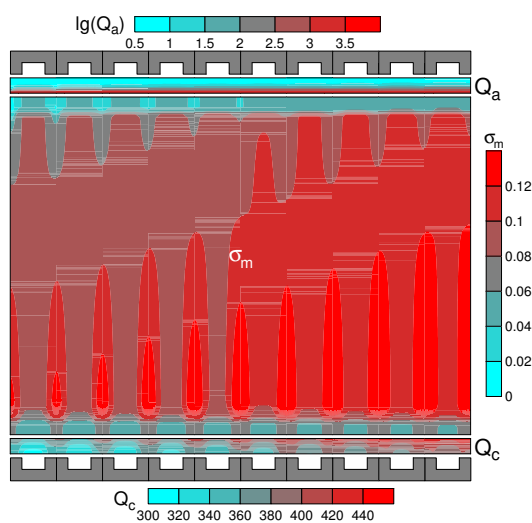
Figure 4 shows maps of reaction rates on both sides and a map of membrane conductivity of the base cell when the mean current density is 200 mA cm^{-2} . Figure 5 shows the same maps for the dry cell.



The same maps as in Figure 4 for a dry cell. The mean current density is 200 mA cm^{-2}

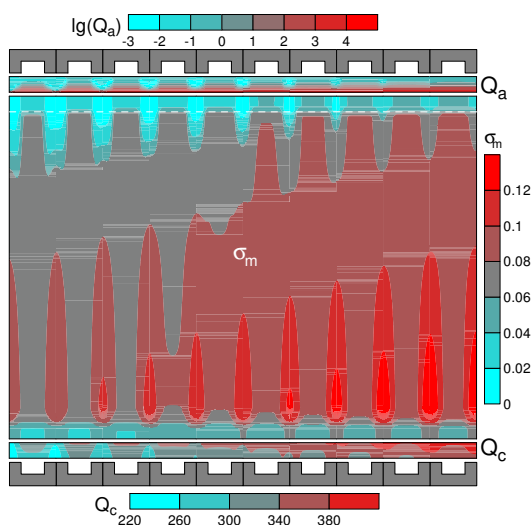
Comparison of these figures shows that in both the cases near the outlet the distribution of parameters is quite similar. Far from the inlet, water is concentrated on the cathode side, in front of the ribs. The reaction rate along with the proton current in the membrane is higher there.

The peculiarity of the dry cell is the formation of water-depleted regions near the inlet on the anode side (in front of the ribs, Figure 5). These regions arise due to the electroosmotic transport of water from the anode to the cathode. The flux of water from the nearest channel windows to these regions is lower than the drainage due to electroosmosis. The local drying of the anode catalyst layer and of bulk membrane destroys the uniformity of reaction rate along the anode channel (Figure 5).

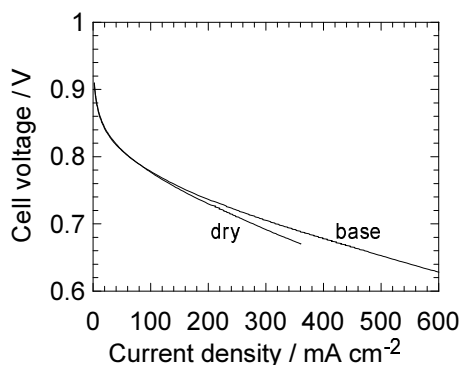


The same maps as in Figure 4 (base cell). The mean current density is 400 mA cm^{-2}

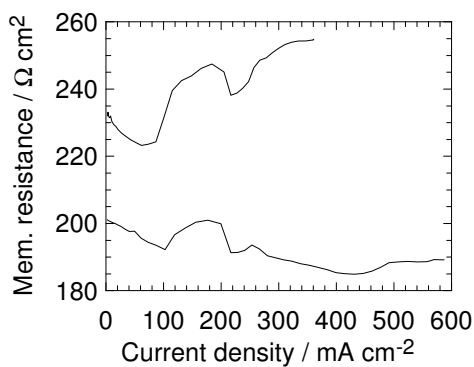
These effects became more pronounced when the mean current density increases. Figures 6 and 7 show the maps of parameters in both the cells for the twice higher mean current density. Comparison of Figures 6 and 7



The same maps as in Figure 4 for a dry cell. The mean current density is 360 mA cm^{-2}



The voltage current curves of the base and dry cells



The membrane resistance in the base and dry cells

shows the catastrophic membrane drying near the inlet of the anode channel in the dry cell.

Figure 8 displays the voltage current curves of both cells. Drying leads to a growth of the membrane resistance (Figure 9), which is the main reason for a worse performance of the dry cell. Note that at low current densities (below $\simeq 250 \text{ mA cm}^{-2}$) the resistances of membranes in both cases vary similarly. However, above 250 mA cm^{-2} the resistance of the base cell decreases with j , whereas the resistance of the dry cell increases.

The results presented clearly demonstrate that a fuel cell is a distributed system. Due to electrochemical reactions, the gas composition in both the anode and cathode channels varies with distance. On the other hand, the distribution of parameters across the MEA in the (x, y) plane is strongly nonuniform (see also [12, 13, 21]). The fuel cell with the conventional flow field is hence essentially a quasi-3D system. The above results demonstrate how the Q3D model locates the MEA regions “dangerous” with respect to drying.

5. Acknowledgments

The simulations were performed on a Cray T3E computer of the Central Institute of Applied Mathematics, Research Center Jülich and on a PC-based cluster at the Research Computing Center of Moscow State University.

List of symbols

c	Feed gas molar concentration (mole cm^{-3})
c_{ref}	Reference molar concentration of feed gas (mole cm^{-3})
D	Overall effective diffusion coefficient (cm^2s^{-1})
D^b	Effective binary diffusion coefficient (cm^2s^{-1})
D^K	Knudsen diffusion coefficient (cm^2s^{-1})
D_w^m	Diffusion coefficient of water in membrane (cm^2s^{-1})
F	Faraday constant (9.6495×10^4 Coulomb g-mole^{-1})
h	Channel height above the backing layer (cm)
i_*	Exchange current density per unit volume (A cm^{-3})
j	Local current density (A cm^{-2})
k^p	Hydraulic permeability (cm^2)
l	Thickness of catalyst layer (cm)
l_{MEA}	Thickness of membrane–electrode assembly (cm)
M	Total molecular weight of gas mixture (g mole^{-1})
M_i	Molecular weight of i th gas component (g mole^{-1})
N	Molar flux (mole $\text{cm}^{-2}\text{s}^{-1}$)
n	Number of electrons participating in electrochemical reaction
n^d	Drag coefficient (number of water molecules transported by proton)
p	Pressure (1.0133×10^6 g $\text{cm}^{-1}\text{s}^{-2}$)
Q	Local rate of electrochemical reaction (A cm^{-3})
R	Gas constant (8.314 J K^{-1} g-mole^{-1} or 8.314×10^7 g $\text{cm}^2\text{s}^{-2}\text{K}^{-1}$ g-mole^{-1})
S	Stoichiometry coefficient
T	Cell temperature (K)
v	Velocity of flow in channel (cm s^{-1})
$v^{\text{D'Arcy}}$	D'Arcy velocity in backing layers (cm s^{-1})
x	Coordinate across MEA (cm)
y	Coordinate along MEA surface (cm)
z	Coordinate along channel (cm)

Greek symbols

α	Transfer coefficient
γ	Order of reaction
Δ_0	Thickness of transition region (cm)
ε^B	Bruggemann correction for porosity
η	Local overpotential (V)
μ	Gas viscosity ($\text{g cm}^{-1}\text{s}^{-1}$)
ξ	Molar fraction
ρ	Density of gas in feed channels (g cm^{-3})
σ_a	Carbon phase conductivity on anode side ($\Omega^{-1} \text{cm}^{-1}$)
σ_c	Carbon phase conductivity on cathode side ($\Omega^{-1} \text{cm}^{-1}$)
σ_m	Membrane phase conductivity ($\Omega^{-1} \text{cm}^{-1}$)
φ	Potential of carbon phase (V)
φ_m	Potential of membrane phase (V)
ψ	Correction factor in expression for Knudsen diffusion coefficient

Subscripts

a	on anode side
c	on cathode side
H_2	hydrogen
i	enumerate gas components
O_2	oxygen
m	membrane phase
w	water vapor

References

1. P. Costamagna and S. Srinivasan, "Quantum jumps in the PEMFC science and technology from the 1960s to the year 2000", *J. Power Sources*, **102**, 1-2: 242-252, 2001.
2. T.F. Fuller and J. Newman, "Water and thermal management in solid-polymer-electrolyte fuel cells", *J. Electrochem. Soc.*, **140**, 5: 1218-1225, 1993.
3. T.V. Nguyen and R.E. White, "A water and heat management model for proton-exchange-membrane fuel cells", *J. Electrochem. Soc.*, **140**, 8: 2178-2186, 1993.
4. J.S. Yi and T.V. Nguyen, "An along-the-channel model for proton exchange membrane fuel cells", *J. Electrochem. Soc.*, **145**, 4: 1149-1159, 1998.
5. K. Dannenberg, P. Ekdunge, and G. Lindbergh, "Mathematical model of the PEMFC", *J. Appl. Electrochem.*, **30** 12: 1377-1387, 2000.
6. S. Um, C.-Y. Wang, and K.S. Chen, "Computational fluid dynamics modeling of proton exchange membrane fuel cells", *J. Electrochem. Soc.*, **147**, 12: 4485-4493, 2000.
7. P. Futerko and I.-M. Hsing, "Two-dimensional finite-element method study of the resistance of membranes in polymer electrolyte fuel cells", *Electrochimica Acta*, **45**: 1741-1751, 2000.
8. I.-M. Hsing and P. Futerko, "Two-dimensional simulation of water transport in polymer electrolyte fuel cells", *Chem. Engineer. Sci.*, **55**: 4209-4218, 2000.
9. Z.H. Wang, C.Y. Wang, and K.S. Chen, "Two-phase flow and transport in the air cathode of proton exchange membrane fuel cells", *J. Power Sources*, **94**: 40-50, 2001.
10. D. Natarajan and T.V. Nguyen, "A two-dimensional, two-phase, multicomponent, transient model for the cathode of a proton exchange membrane fuel cell using conventional gas distributors", *J. Electrochem. Soc.*, **148**, 12: A1324-A1335, 2001.
11. S. Dutta, S. Shimpalee, and J.W. Van Zee, "Three-dimensional numerical simulation of straight channel PEM fuel cells", *J. Appl. Electrochem.*, **30**: 135-146, 2000.
12. A.A. Kulikovskiy, "Numerical simulation of a new operational regime for a polymer electrolyte fuel cell", *Electrochem. Comm.*, **3**, 8: 460-466, 2001.
13. A.A. Kulikovskiy, "Quasi three-dimensional modeling of a PEM fuel cell: Comparison of the catalyst layers performance", *Fuel Cells*, **1**, 2: 162-169, 2001.
14. F. Büchi and G.G. Scherer, "Investigation of the transversal water profile in Nafion membranes in polymer electrolyte fuel cells", *J. Electrochem. Soc.*, **148**, 3: A183-A188, 2001.
15. A.A. Kornyshev and A.A. Kulikovskiy, "Characteristic length of fuel and oxygen consumption in feed channels of polymer electrolyte fuel cells", *Electrochimica Acta*, **45**, 28: 4389-4395, 2001.
16. R.B. Bird, W.E. Stewart, and E.N. Lightfoot, *Transport Phenomena*, New York: Wiley, 1960.
17. A.A. Kulikovskiy, "Modeling of water management in polymer electrolyte fuel cells", *J. Electrochem. Soc.*, 2002, (submitted).
18. A.A. Kulikovskiy, "Gas dynamics in channels of a gas-feed direct methanol fuel cell: Exact solutions", *Electrochem. Comm.*, **3**, 10: 572-79, 2001.
19. D.L. Scharfetter and D.L. Gummel, "Large signal analysis of a silicon read diode oscillator", *IEEE Trans. on Electr. Devices*, ED-16: 64-77, 1969.
20. A.A. Kulikovskiy, "Simple and accurate scheme for nonlinear convection-diffusion equations", *J. Comp. Phys.*, **173**, 2: 716-729, 2001.
21. A.A. Kulikovskiy, J. Divisek, and A.A. Kornyshev, "Modeling the cathode compartment of polymer electrolyte fuel cells: Dead and active reaction zones", *J. Electrochem. Soc.*, **146**, 11: 3981-3991, 1999.
22. A.A. Kulikovskiy, J. Divisek, and A.A. Kornyshev, "Two-dimensional simulation of direct methanol fuel cells: A new (embedded) type of current collectors", *J. Electrochem. Soc.*, **147**, 3: 953-959, 2000.

Поступила в редакцию
09.07.2002